
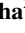




JGR Solid Earth

RESEARCH ARTICLE

10.1029/2023JB027877

Glacier Melting Triggers Massive Gravel Deposition in Central Italy's River Basins, Unveiling Deglacial Events From 1250 to 780 ka

F. Florindo¹ , F. Marra¹ , B. R. Jicha² , F. Bulian³, A. Di Chiara¹ , and P. Srivastava^{1,4} 

¹Istituto Nazionale di Geofisica e Vulcanologia, Rome, Italy, ²Department of Geoscience, University of Wisconsin-Madison, Madison, WI, USA, ³Groningen Institute of Archaeology, Groningen, The Netherlands, ⁴Indian Institute of Geomagnetism, Navi Mumbai, India

Key Points:

- We provide ⁴⁰Ar/³⁹Ar and paleomagnetic constraints to seven aggradational successions recovered from a 120 m deep borehole in Rome
- Each aggradational succession is correlated with a period of sea-level rise encompassing MIS 37 through MIS 19, 1250 to 780 ka
- This study shows that gravel deposition in the catchment basin of the main rivers in central Italy is a direct proxy of deglacial events

Supporting Information:

Supporting Information may be found in the online version of this article.

Correspondence to:

F. Florindo,
fabio.florindo@ingv.it

Citation:

Florindo, F., Marra, F., Jicha, B. R., Bulian, F., Di Chiara, A., & Srivastava, P. (2024). Glacier melting triggers massive gravel deposition in central Italy's river basins, unveiling deglacial events from 1250 to 780 ka. *Journal of Geophysical Research: Solid Earth*, 129, e2023JB027877. <https://doi.org/10.1029/2023JB027877>

Received 20 SEP 2023

Accepted 19 FEB 2024

Author Contributions:

Conceptualization: F. Marra

Investigation: F. Florindo, B. R. Jicha

Supervision: F. Marra

Writing – original draft: F. Florindo,

F. Marra, A. Di Chiara, P. Srivastava

Writing – review & editing: F. Florindo,

F. Marra, B. R. Jicha, F. Bulian, A. Di

Chiara, P. Srivastava

Abstract The purpose of this study was to prove the direct correlation of a successions of gravel-clay beds recovered in borehole with the melt-water pulses associated with the sea-level oscillations indicated in the $\delta^{18}O$ record in the time-span preceding the 100-kyr glacial cycles. Aimed at this scope, we provide combined ⁴⁰Ar/³⁹Ar and paleomagnetic constraints to a set of seven aggradational successions recovered from a 120 m deep borehole drilled in the buried Paleo-Tiber delta in Rome (central Italy). The geochronologic constraints enable the correlation of each aggradational succession, characterized by a sudden transition from coarse gravel at the base to sandy clay sediments, with periods of sea-level rise indicated by the $\delta^{18}O$ curve encompassing MIS 37 through MIS 19, from 1250 to 780 ka. This stratigraphy, provides a unique and unprecedented well-dated evidence of glacial/deglacial events, matching the global benthic $\delta^{18}O$ stack during this time frame.

Furthermore, this study validates the hypothesis that gravel deposition in the catchment basin and the delta of the main rivers in central Italy is triggered by the melting of glaciers in the Apennines Mountain range. It demonstrates the significant potential of these deglaciation proxies to be used worldwide to unravel the chronology of glacio-eustatic events.

Plain Language Summary In this study, we used a combination of dating techniques and paleomagnetic data to examine a series of sediment layers found in a buried ancient river delta in Rome, Italy. These sediment layers were collected from a 120 m deep borehole. By analyzing the age of these sediment layers, we were able to link them to a period in the past when sea level was rising. This sea-level rise occurred between 1250 and 780 ka, covering a range of time from MIS 37 to MIS 19. These sediment layers show a distinct change from coarse gravel to sandy clay, which provides valuable information about glacial and deglacial events. These findings support the idea that the deposition of gravel in river catchment areas and deltas in central Italy is linked to the melting of glaciers in the Apennines Mountain range. This research not only validates this hypothesis but also highlights the potential for using similar techniques globally to better understand the timing of glacio-eustatic events.

1. Introduction

The coarse clastic sediments found at the base of the aggradational successions of the (paleo-) rivers in central Italy, consisting of gravel with a grain size between >1 and <10 cm, have been identified as evidence of global deglacial events occurred during the Pleistocene (Giaccio et al., 2021; Marra et al., 2022). According to the sedimentary model proposed by Marra et al. (2008, 2016), the transportation of coarse gravel from the Apennine Mountain chain through the (Paleo-) Tiber River channel, and its subsequent accumulation on the Tyrrhenian Sea coast, is only possible during glacial terminations due to several factors that occur simultaneously.

1. Rapid melting of Apennine glaciers leading to an increased supply of sediment to the drainage basin;
2. Increased regional rainfall;
3. Lowered sea levels at the onset, causing a steeper gradient and greater river transport capacity;
4. A fast sea level rise, leading to a sudden drop in gradient and transport capacity, and ultimately the accumulation of coarse material within the fluvial channels.

Recent studies have provided evidence that these principles also apply to the upper parts of the Tiber River catchment basin, extending as far as 100 km inland (Giaccio et al., 2021; Marra, Costantini, et al., 2019). Similar

© 2024. The Authors.

This is an open access article under the terms of the [Creative Commons](https://creativecommons.org/licenses/by/4.0/)

[Attribution-NonCommercial-NoDerivs](https://creativecommons.org/licenses/by/4.0/)

License, which permits use and distribution in any medium, provided the original work is properly cited, the use is non-commercial and no modifications or adaptations are made.

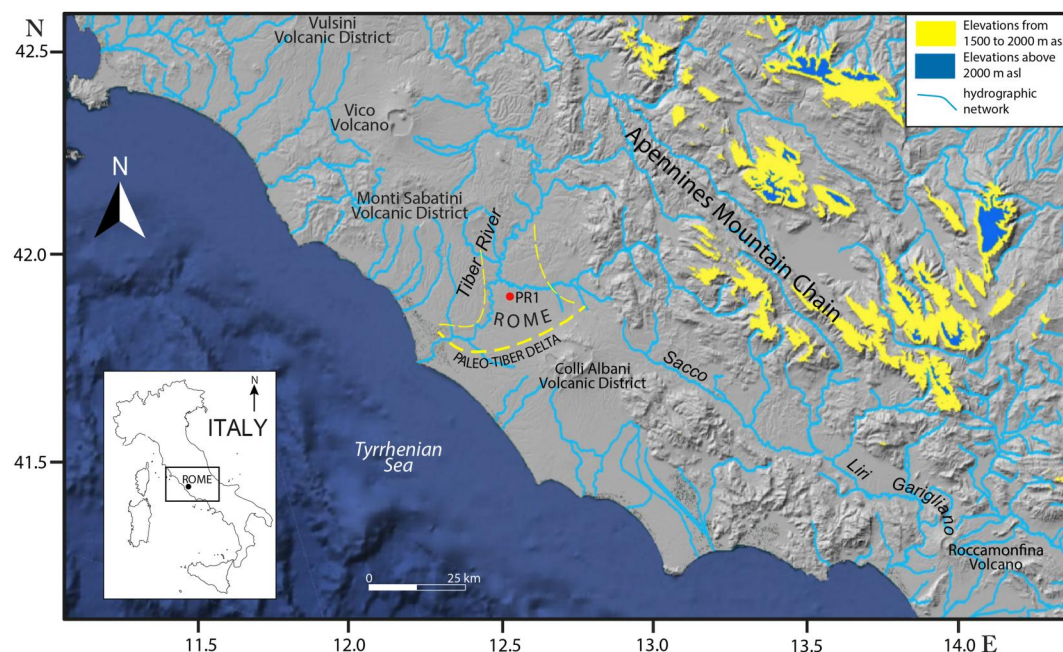


Figure 1. Shaded relief map of central Italy displaying the drainage basins of the Tiber and Sacco-Liri-Garigliano Rivers, along with the location of the PR1 borehole. Areas exhibiting evidence of glacial landforms associated with MIS 14 through MIS 6 glaciations, as outlined by Giraudi and Giaccio (2017), are highlighted. Glacial landforms related to the Apennine glaciers have been documented at elevations as low as 1500 m above sea level.

patterns have been observed in other hydrographic basins in central Italy that extend to the Apennine divide, where glaciers existed during the Pleistocene glacial periods (Giraudi & Giaccio, 2017). For example, the Sacco-Liri-Garigliano Rivers exhibit a similar sedimentary record (Marra et al., 2022) (Figure 1).

The sedimentary model proposed by Marra et al. (2008, 2016) was developed using $^{40}\text{Ar}/^{39}\text{Ar}$ dating of volcanic layers embedded within the sedimentary successions, along with conducting a paleomagnetic investigation of the clay sections. This strategy enabled the depiction of a chronological interconnection with the $\delta^{18}\text{O}$ record (Alvarez et al., 1996; Florindo & Marra, 1995; Karner & Marra, 1998; Karner & Renne, 1998; Marra et al., 1998). A series of 13 stacked aggradational successions has been developed over the last years. These successions were created by correlating various aggradational sections cropping out on the Tyrrhenian Sea margin using different geochronological constraints. More than fifty $^{40}\text{Ar}/^{39}\text{Ar}$ and ^{14}C dates, as shown in Figure 2, were utilized. This extensive analysis has demonstrated that these sedimentary successions were deposited during fast sea-level rises (melt-water pulses) leading to the warm peaks, or highstands, in the $\delta^{18}\text{O}$ record (Florindo et al., 2007; Giaccio et al., 2021; Karner & Marra, 2003; Marra & Florindo, 2014; Marra, Costantini, et al., 2019; Marra et al., 2008, 2015, 2016, 2017, 2021; Pereira et al., 2020; Villa et al., 2016). In particular, Marra et al. (2013, 2016) have shown that the aggradational successions of the Paleo-Tiber and the Modern Tiber River exhibit an abrupt change in grain size, shifting from coarse gravel ($1 < \phi < 10$ cm) to sandy clay ($\phi \leq 1$ mm) sediments. This change coincides with the occurrence of melt-water pulses during glacial terminations, while the deposition of the thick fine-grained sedimentary section matches the establishment of the sea-level highstand (Figure 2).

This sedimentary model is highly sensitive and can even detect minor melt-water pulses. For instance, early aggradational phases corresponding to moderate sea-level oscillations preceding the main melt-water pulse have been identified using $^{40}\text{Ar}/^{39}\text{Ar}$ methods. These phases lead to the isotopic highstand during glacial terminations V (MIS 12-11), IV (MIS 10-9), and III (MIS 8-7) (Giaccio et al., 2021; Marra et al., 2016, 2022) (see Figure 2b). Giaccio et al. (2021) and Marra et al. (2022) have identified a significant correlation between melt-water pulse events in the $\delta^{18}\text{O}$ record, peaks in the ice-rafted debris (IRD) record (Barker et al., 2019), and the deposition of gravel beds at the base of the aggradational successions. This correlation suggests that the deposition of gravel in the catchment basins of the Tiber and Sacco-Liri-Garigliano Rivers represents a reliable proxy for deglaciation events. By combining radioisotopically dated (^{14}C and $^{40}\text{Ar}/^{39}\text{Ar}$) morpho-sedimentary units, this composite

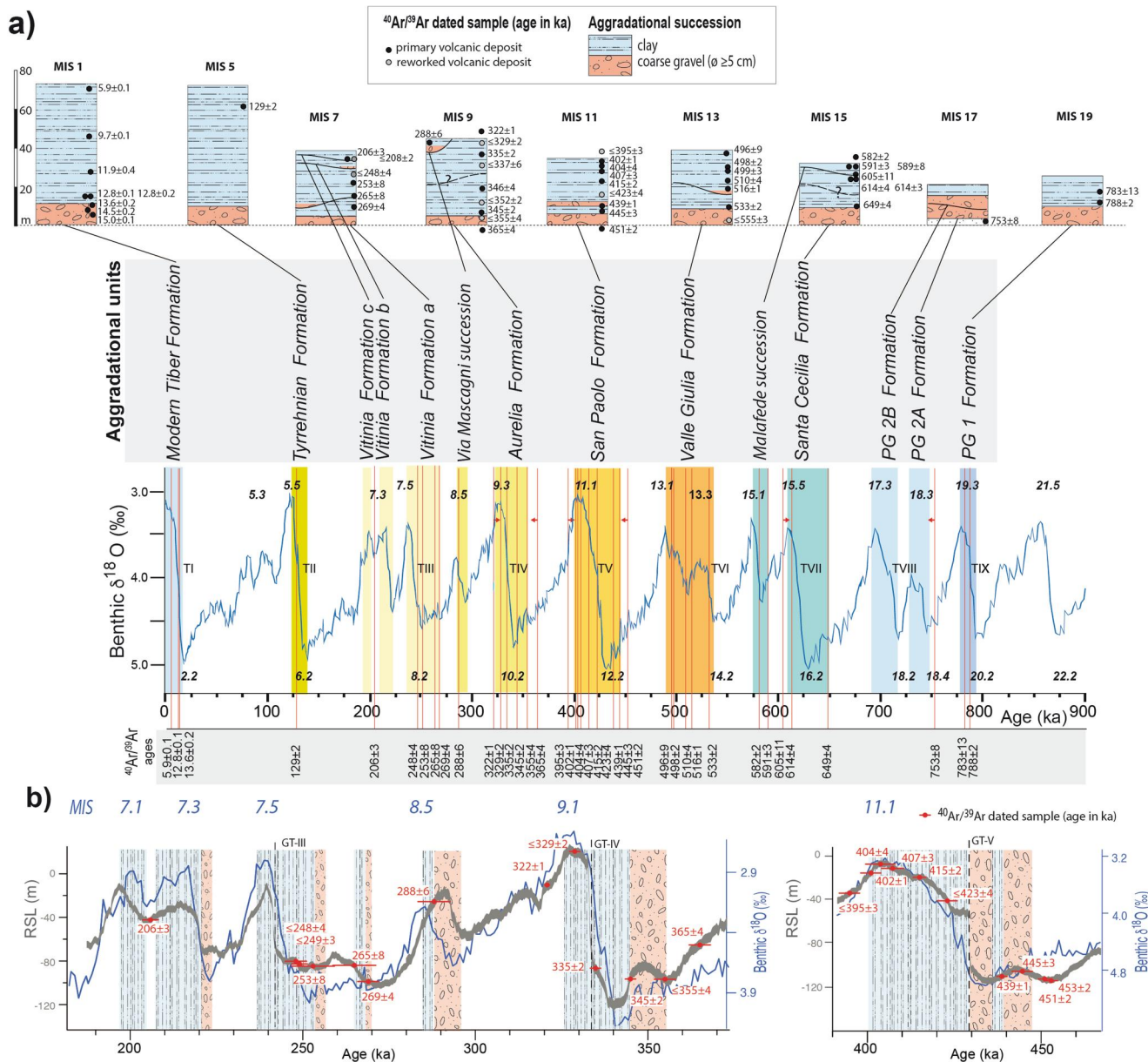


Figure 2. (a) Stacked aggradational successions of the Paleo-Tiber River and geochronologic constraints achieved in previous literature (see text for full references), allowing for their correlation with the oxygen isotope record. (b) Examples of chronostratigraphic constraints provided by the aggradational successions correlated with MIS 7.1 through MIS 9.3 and with MIS 11.1, highlighting the occurrence of early aggradational phases corresponding to moderate sea-level oscillations in the Relative Sea Level curve by Grant et al. (2014).

record can provide crucial geochronological constraints that are often lacking in Middle Pleistocene sea-level records, thus contributing to a better understanding of the relationship between insolation changes and sea-level oscillations.

To investigate these sedimentary layers, a deep borehole (PR1, Figures 3 and 4) was drilled in Rome, reaching a depth of 120 m. This borehole aimed to recover a succession of gravel and clay horizons that were not visible in outcrop. The identification of these horizons was based on stratigraphic logs from the 1950s (see Figure S1 in Supporting Information S1), which were conducted during the past decades by the Municipal agency for electricity and environment (ACEA) for hydrogeological purposes. These logs were stored in the databank of the Istituto Nazionale di Geofisica e Vulcanologia (INGV) and had not been previously published. Earlier shallow boreholes carried out by INGV had already retrieved the upper gravel

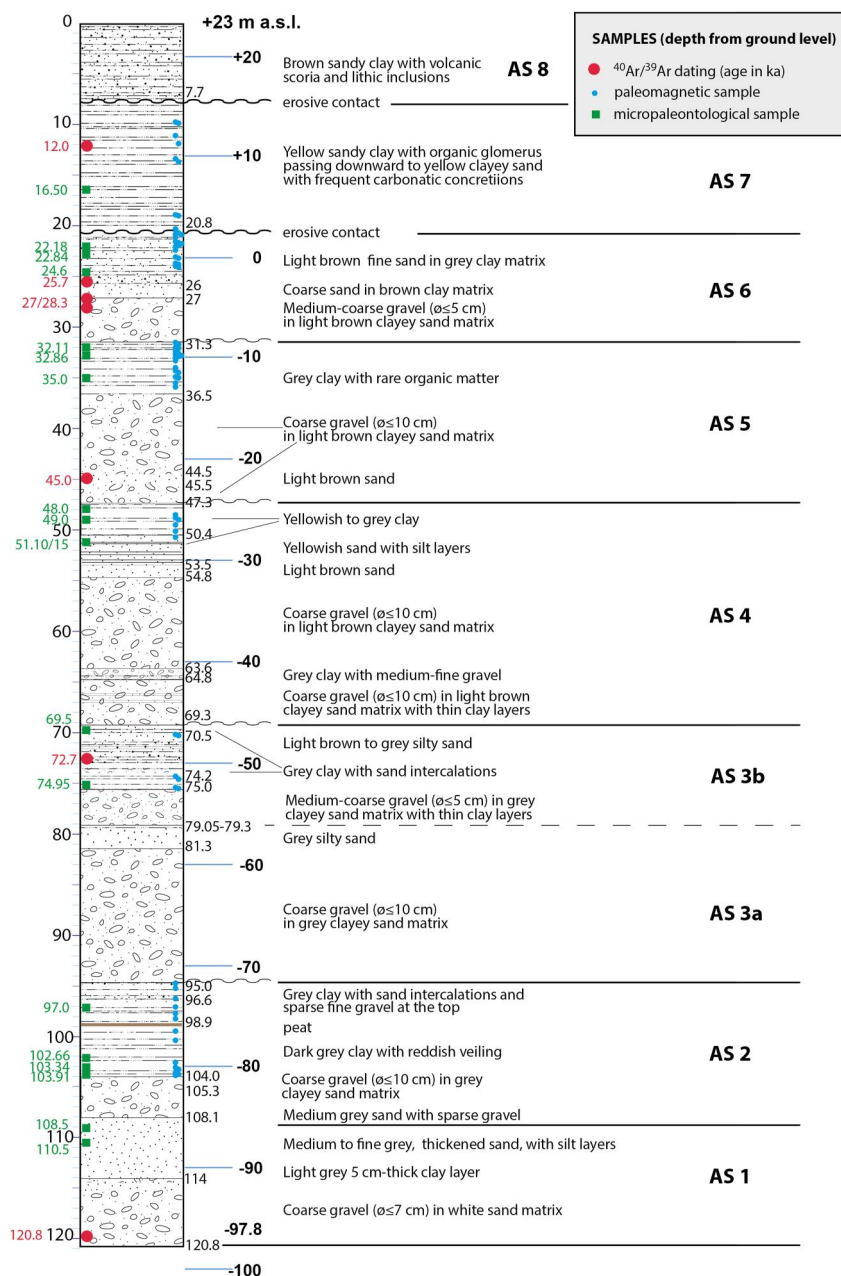


Figure 3. Stratigraphic log of borehole PR1 showing the boundaries of the aggradational successions and the sampling. See text for comments and explanation.

layer of this succession, which was dated between 783 and 802 ka using paleomagnetic investigation techniques (Florindo et al., 2007) and correlation with $^{40}\text{Ar}/^{39}\text{Ar}$ dated tephra layers in nearby boreholes. Florindo et al. (2007) associated this gravel layer with glacial termination IX at the beginning of Marine Isotope Stage (MIS) 19. The purpose of the PR1 borehole was to recover the >800 ka gravel-clay horizons in order to provide geochronologic constraints that directly correlate with the sea-level oscillations indicated in the $\delta^{18}\text{O}$ record. Our investigation involved paleomagnetic analysis of the recovered clay horizons, $^{40}\text{Ar}/^{39}\text{Ar}$ dating of loose sanidine crystals extracted from the sand matrix of gravel layers (detrital sanidine), and micropaleontological analysis of selected samples.

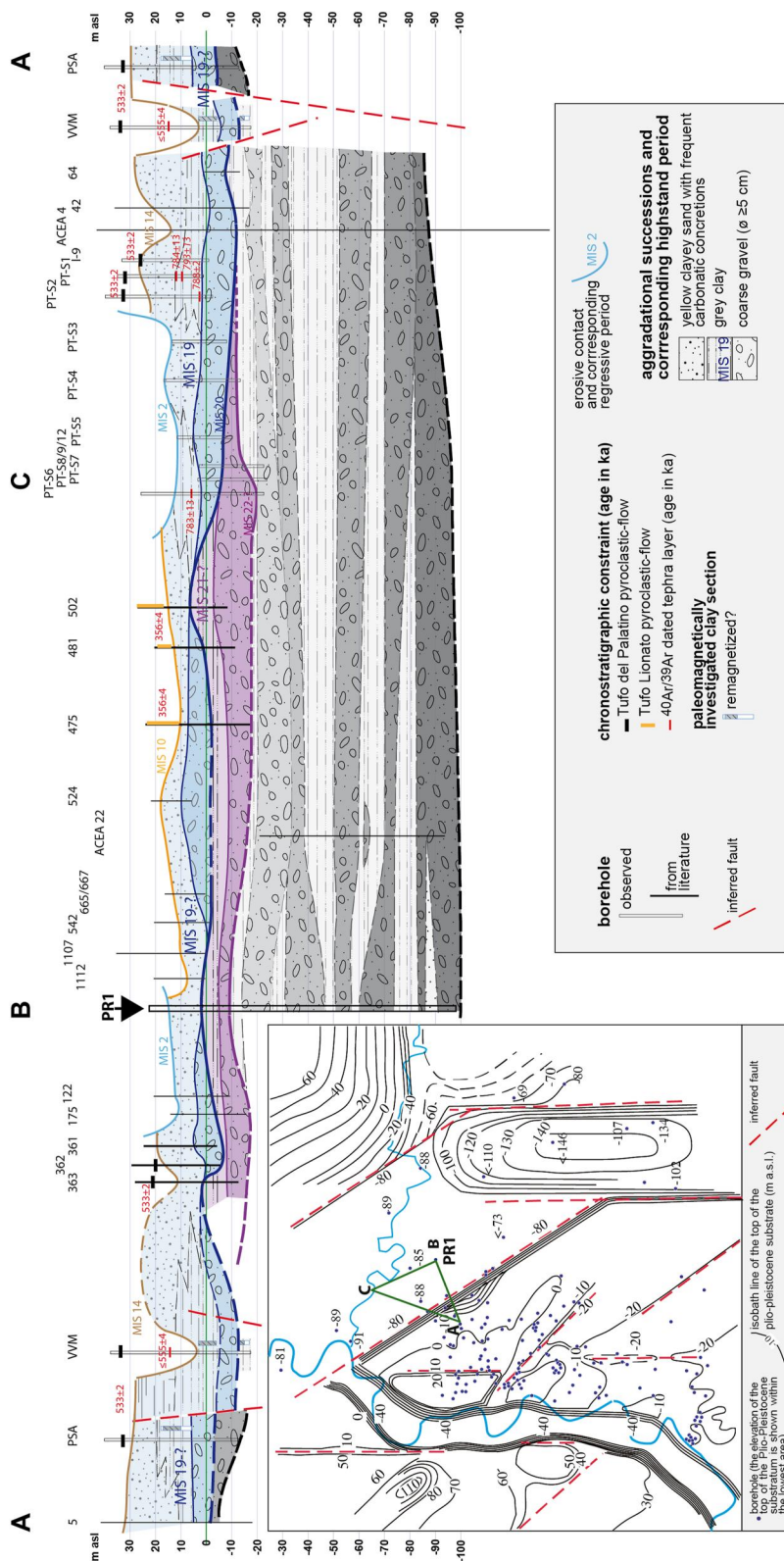


Figure 4. A tentative correlation is presented among the various aggradational successions identified in the previously drilled boreholes in Rome and the PR1 borehole. The inset provides a visualization of the reconstructed trend of the Plio-Pleistocene marine substrate, based on data from deep boreholes, along with the inferred faults affecting the substrate. This figure has been modified from Marra and Florindo (2014).

2. Methods

2.1. Stratigraphic and Sedimentologic Analysis

One defining characteristic of the aggradational successions of the Paleo-Tiber River is the sudden shift in sedimentary facies between the lower and upper sections of the sedimentary record (Giaccio et al., 2021; Marra et al., 2008, 2013, 2016, 2022). This is also observed in the 120-m-thick succession extracted from the PR1 borehole, where a sharp boundary separates a layer of well-rounded limestone and chert pebbles, with diameters reaching up to approximately 10 cm (as measured by the core's inner diameter), embedded in a matrix of silty sand (0.5–1.0 mm), from a separate layer of mostly clayey <0.004 mm and sandy <0.5 mm sediments that is several meters thick (5–9 m, as shown in Figure 3 and Figures S2 to S8 in Supporting Information S1). Notably, no clastic particles larger than 2 mm are ever found in the upper sedimentary layer above this boundary. Given the clarity of this boundary, which allows for objective identification, detailed granulometric and sedimentologic analyses are beyond the scopes of the present study and are not included here. Based on the conceptual model of aggradational successions proposed by Marra et al. (2008, 2016), the sharp sedimentary boundaries are used as a proxy for glacial terminations. The lower coarse sedimentary package is believed to indicate the glacial lowstand, which includes the erosive phase that corresponds to a sedimentary hiatus (unconformity surface at the base of each gravel layer) and the initial sea-level rise at the end of the glacial maximum, which leads to the rapid accumulation of gravel. The fine-grained package above the sedimentary boundary is believed to indicate the establishment of the sea-level highstand during the interglacial period. In order to investigate the depositional environmental and paleogeographic context and support the inferences on the sea-level oscillations, micropaleontologic analysis was performed on samples collected from the clay sections.

2.2. Micropaleontologic Analysis

A 20–40 g fraction was chosen from each one of the 18 samples analyzed for micropaleontological content, then oven dried and soaked in water before being sieved over a >63 μm and >125 μm mesh sieve. The resulting fractions (<63 μm , 63–125 μm and >125 μm) were separated by weighing the sieve refuse and expressing it as a percentage. Due to the low number of specimens, a qualitative analysis was performed on the >125 μm residue, and the main benthic foraminifer species were identified. For planktic foraminifers, only their presence or absence was noted. These microfossils are useful biological indicators that allow for the paleoenvironmental characterization of the sediments at the time of deposition (Kucera, 2007; Van der Zwaan et al., 1999).

2.3. $^{40}\text{Ar}/^{39}\text{Ar}$ Analysis

Since primary volcanic layers were not present in the sedimentary deposits recovered from borehole PR1, we utilized the detrital sanidine method to determine the maximum age of these deposits (Heizler et al., 2021; Marra et al., 2022; Marra, Gaeta, et al., 2019). Additionally, we re-dated a new sample of the primary pumice fallout recovered from borehole PT2 which was previously dated at $802 \pm 4\text{ka}$ (Florindo et al., 2007; Karner et al., 2001). Sanidine phenocrysts were extracted from both the primary pumice and from six sedimentary samples. These samples were then co-irradiated with the 1.1864 Ma Alder Creek sanidine standard (Jicha et al., 2016) at the Oregon State University TRIGA reactor in the Cadmium-Lined In-Core Irradiation Tube. The single crystal fusion analyses were conducted at the WiscAr laboratory at the University of Wisconsin-Madison, utilizing a 55W CO_2 laser and a Noblesse multi-collector mass spectrometer, according to (Jicha et al., 2016). The full analytical data are reported in Data Set S1.

2.4. Paleomagnetic Sampling, Laboratory Procedures, and Analysis

We collected 82 samples of core PR1 using standard plastic cubes with a volume of approximately 8 cm^3 . We obtained a total of 80 samples from the core's center, at depths ranging from 9.85 to 103.85 m. All samples were carefully oriented with respect to vertical; lack of azimuthal orientation did not pose a problem for polarity determination because the geomagnetic field at the latitude of this site ($41^\circ 53'\text{N}$) has a steep inclination (± 61 assuming a geocentric axial dipole field). To ensure minimal sample dehydration and alteration, we placed the samples in sealed bags and stored them in a refrigerated room until processing at the Istituto Nazionale di Geofisica e Vulcanologia (INGV) in Rome. At the laboratory, we measured both natural and artificial magnetizations of the samples at room temperature using a narrow-access pass through a 2-G Enterprises cryogenic magnetometer, housed in a shielded room. To demagnetize the samples, we used three mutually orthogonal

alternating field (AF) demagnetization coils that were arranged in-line with the cryogenic magnetometer. We applied successive peak AFs of 0, 4, 8, 13, 17, 21, 25, 30, 35, 40, 45, 50, 60, 80, and 100 mT. To assess the stability of the natural remanent magnetization (NRM), we used vector component diagrams. We determined characteristic remanent magnetization (ChRM) directions by using principal component analysis (PCA) with linear best fits calculated from four or more demagnetization steps (Kirschvink, 1980), using the PuffinPlot paleomagnetic analysis application developed by Lurcock and Florindo (2019).

For each sample, we utilized two options for PCA analysis: (a) the free option, where the line is fitted through the data without the constraint of passing through the origin of orthogonal demagnetization diagrams, and (b) the anchored option, where the line is also fitted through the data but is anchored to the origin of orthogonal demagnetization diagrams. Case-by-case, we decided on the most appropriate approach.

After demagnetizing the NRM of the samples, a series of rock magnetic analyses were performed to determine changes in magnetic mineral composition, concentration, and grain size throughout the core. Low-field magnetic susceptibility (χ) was measured using an AGICO KLY-2 Kappabridge magnetic susceptibility meter, with a 0.1 mT field at a frequency of 470 Hz. An anhysteretic remanent magnetization (ARM) was generated by applying a 0.05 mT direct current (DC) bias field superimposed on a 100 mT peak AF, while moving the samples through the AF and DC coil system at a speed of 10 cm/s, the lowest speed permitted by the control software. The resulting ARM was then measured. Hysteresis loop, backfield demagnetization curves, temperature-dependent magnetic susceptibility (k-T) and first-order reversal curves (FORCs) were among the measurements carried out on 15 samples selected from the clay-rich horizons. Details of the laboratory procedures and analysis are reported in Supporting Information S1.

3. Results

3.1. PR1 Borehole Stratigraphy and Stratigraphic Correlations

The sedimentary succession recovered from borehole PR1 is described in the stratigraphic log of Figure 3. Photograph of the complete set of cores recovered by the drilling are provided in Supporting Information S1. Based on the principles outlined in Section 2.1, a total of six complete and two partially preserved (upper portion) aggradational successions (AS 1–8) have been identified. Except for the uppermost interval, which represents the fine-grained portion of the most recent glacio-eustatic cycle (0.018 ka–Present), corresponding to the alluvial deposits of the Modern Tiber Formation, all the aggradational successions between –120 and 7.7 m can be attributed, in first analysis, to the Paleotiber Succession. This succession encompasses the glacio-eustatic cycles older than 600,000 years (Luberti et al., 2017). Consistently, the basal gravel layers within these aggradational successions show lateral correlation with the gravel layers encountered in the deep ACEA drillings, which were associated with the Paleotiber Succession (Florindo et al., 2007; Marra & Florindo, 2014) (see Figure 4 and Figure S1 in Supporting Information S1). The upper portion of the lowest aggradational succession, AS 1, is characterized by a relatively coarser grain size with compared to the other AS's. It is characterized by intervals of medium to fine sand and silt intervals instead of clay. However, the distinct change in grain size at the top of the basal coarse gravel bed, above which no sediment with a grain size greater than 2 mm is found, aligns with the criteria used to define proxies for glacial terminations in the sedimentary model. Similarly, we have split the AS 3 in two sub-sections AS 3a and AS 3b, based on the occurrence of a 2 m-thick layer of silty sand within the very thick gravel bed recovered between depths of –75 and –95 m. Two additional “canonical” aggradational successions, AS 4 and AS 5, are observed between depths of –31.3 and –69.3 m. These successions are characterized by a sharp transition from coarse gravel to fine sand and clay. A noticeable color change from gray to light brown is also observed in the sand and minor clay fraction within the matrix of the coarse gravel beds, starting from AS 4 (see Supporting Information S1 for photographs of the cored sediments). The upper portion of AS 6, which consists of fine-grained sediments, exhibits a higher abundance of sand fraction and an overall light brown color. A distinct unconformity is observed at the top of this sandy clay horizon, indicating erosional contact with the overlying sediments of AS 7. AS 7 is characterized by a distinctive package of yellow to whitish clayey sand, frequently containing carbonate concretions and travertine layers. In previous literature, this package was referred to as the Paleotiber 2b Unit (e.g., Marra & Rosa, 1995) and later as the Paleotiber 3 Unit (Florindo et al., 2007). This sedimentary horizon overlays the Paleotiber 2 Unit, which has been correlated through $^{40}\text{Ar}/^{39}\text{Ar}$ dating and paleomagnetic analysis with MIS 19 (Florindo et al., 2007) (see Figure 4).

Based on these preliminary correlations, an age of over 800 ka is inferred for AS 1 through AS 6, which were recovered in the PR1 borehole. Figure 4 presents the A-B-C profile, illustrating the lateral correlation of the MIS 19 aggradational succession and the overlying sandy-travertine horizon across the subsurface of Rome, including the borehole PR1. This correlation is based on observations from various boreholes and stratigraphic logs available in the INGV databank. The AS represented by the underlying gravel-and-clay sedimentary package in the cross-section of Figure 4 is tentatively correlated with MIS 21, while the lower aggradational successions within the Paleotiber Graben are indicated in shades of gray. The inset map in Figure 4 illustrates the trend of the marine clay substrate (Marne Vaticane Formation (Marra et al., 1995)) in the Rome area, along with the inferred buried faults surrounding the tectonic depression where these alternating gravel and clay horizons are found. The presence of this area, influenced by tectonic and erosional processes, is inferred by comparing the base level of the continental gravel beds (at approximately 100 m below sea level) with the base level of the 800 ka-old gravel bed and the overlying coastal clay deposit of the Ponta Galeria Formation 1. In the southwestern area of Rome, the Ponta Galeria Formation 1 occurs between 10 and 35 m above sea level and correlates with the MIS 19 aggradational succession in Rome, which occurs between -10 and 15 m above sea level (Florindo et al., 2007; Marra et al., 1998; Marra & Florindo, 2014). However, due to the lack of geochronological data on the deeper gravel beds, information regarding the tectonic rate and the timing of gravel accumulation is currently unavailable.

3.2. Micropaleontological Data

Results of micropaleontological analyses are summarized in Table 1. A detailed discussion of the environmental context is provided in Section 4.

3.3. $^{40}\text{Ar}/^{39}\text{Ar}$ Age Data

Results of single crystal dating of the sedimentary samples collected in PR1 and the primary fallout pumice collected in PT-S2 boreholes are shown in Figure 5.

Full $^{40}\text{Ar}/^{39}\text{Ar}$ data are in Data Set S1.

3.3.1. Sample PT2-S2B

Twenty-seven sanidine crystals extracted from pumice clots of this primary tephra yielded a weighted mean age of 787.6 ± 1.9 ka (2σ), superseding previous, less constrained age assessment of 802.4 ± 2.9 ka (1σ), which was based only on 6 crystals (Florindo et al., 2007). The new age is in excellent agreement with the astrocalibrated age of glacial termination IX at the onset of MIS 19 (ca. 790 ka (Lisiecki & Raymo, 2005)), and provides new support to the sedimentary model of the aggradational successions. Indeed, sample PT2-SB occurred few cm above the gravel-clay transition marking the glacial termination in borehole PT-S2 (Figure 5).

3.3.2. Sample PR1-12

A large youngest population of 22 crystals extracted from this sedimentary sample yielded a weighted mean age of 807.4 ± 1.4 ka (2σ), whereas 7 other crystals yielded scattered ages ranging 823–867 ka. Notably, with respect to the underlying samples in which ages younger than 1.3 Ma are lacking, sample PR1-12 marks the beginning of the alkaline-potassic volcanic activity of the Roman Magmatic Province (Peccerillo, 2017), and references therein) since ca. 810 ka, as documented in the mid (Marra & Florindo, 2014) and distal (Giaccio et al., 2015) tephrostratigraphic settings. However, scant eruptive activity occurred in the interval 870–810 ka is evidenced by sample PR1-12, whereas no dates in the interval 0.87–1.31 Ma are found in the underlying samples PR1-25 and PR1-27/28.3, which are inferred to have an age of ca. 870 ka (i.e., glacial termination x; see ahead).

3.3.3. Samples PR1-25.7, PR1-27/28.3, PR1-45.0, PR1-72.7, PR1-120.8

All these samples yielded a single, very homogeneous crystal population ranging 1318.6 ± 2.0 – 1311.1 ± 1.5 ka, providing a maximum age for the AS1 through AS6. This age matches that of the Mount Cimino volcanic activity (Barberi et al., 1994) and the limited age range displayed by the five samples should be considered to represent that of an intense eruptive activity that occurred in a concentrated time span at this volcanic district. The ages do not overlap at 2σ , but the difference in age between some of the samples is not expected to reflect actual difference in time of deposition of the sediment.

Table 1
Summary of Micropaleontological Data

Sample	Sand (%)	Micropaleontological content	Environment
PR1-16.5	34.58	Barren. Carbonatic concretions are present.	Fluvial environment.
PR1-22.18	39.15	Planktic species: <i>Globigerina bulloides</i> , <i>Turborotalia quinqueloba</i> , <i>Neogloboquadrina pachyderma</i> ; Benthic species: <i>Cibicides lobatulus</i> , <i>Ammonia tepida</i> , <i>Uvigerina mediterranea</i> .	Shallow coastal environment.
PR1-22.84	42.30	Very rare planktic species: <i>G. bulloides</i> , <i>N. pachyderma</i> .	Shallow coastal environment.
PR1-24.6	72.66	Barren	Continental/fluviial environment.
PR1-32.11	6.54	Barren	Continental environment.
PR1-32.86	0.51	Rare ostracods, broken bivalves and some gastropod opercula.	Coastal marsh/peatland environment.
PR1-35.0	3.27	Rare ostracods, broken bivalves and some gastropod opercula.	Coastal marsh/peatland environment.
PR1-48.0	20.47	Very few planktonic species: <i>G. bulloides</i> , <i>N. pachyderma</i> , <i>Globorotalia margaritae</i> , <i>Globorotalita rubescence</i> . Benthic species: <i>A. tepida</i> , <i>C. lobatulus</i> , <i>Asterigerina planorbis</i> , <i>Brizalina</i> spp., <i>Gyroidina</i> spp. <i>Eggerella bradyi</i> , <i>Cybicides</i> sp., <i>Rosalina bradyi</i> , <i>Bulimina aculeata</i> , <i>Nonion commune</i> , <i>Cassidulina laevigata</i> . Some ostracod shells.	Shallow coastal environment.
PR1-49.0	14.79	Rare planktonic species: <i>G. bulloides</i> , <i>N. pachyderma</i> ; Benthic species: <i>Brizalina</i> spp., <i>Adelosina</i> spp., <i>Cassidulina</i> spp., <i>Bulimina</i> spp.	Shallow coastal environment.
PR1-51.10/15	15.57	Planktic species: <i>G. bulloides</i> ; Benthic species: <i>A. beccarii</i> , <i>Cibicides</i> sp..	Transitional environment.
PR1-69.5	4.59	Very rare planktic species: <i>N. pachyderma</i> , <i>G. bulloides</i> . Benthic species present: <i>Kareriella bradyi</i> ., <i>Cibicoides</i> spp., <i>Pullenia bulloides</i> , <i>Brizalina</i> spp..	Shallow water coastal environment.
PR1-74.95	20.47	Planktic species: <i>G. bulloides</i> , <i>N. pachyderma</i> . Benthic species: <i>C. lobatulus</i> (the most present), <i>Nodosaria</i> spp., <i>Bulimina aculeata</i> , <i>C. laevigata</i> (second most abundant), <i>Pullenia bulloides</i> , <i>Cibicides</i> sp., <i>A. beccarii</i> .	Shallow water coastal environment.
PR1-97.0	7.65	Rare planktic species: <i>G. bulloides</i> , <i>Turborotalia quinqueloba</i> , <i>Globigerinita glutinata</i> , <i>N. pachyderma</i> ; Benthic species: <i>Bulimina elongata</i> , <i>Valvulinera bradyana</i> , <i>Cibicoides</i> sp., <i>Melonis</i> spp., <i>Asterigerina planorbis</i> .	Littoral environment.
PR1-102.66	0.46	Benthic very rare species: <i>C. lobatulus</i> and <i>Elphidium</i> spp., Some rare ostracods tests are as well present	Shallow coastal environment.
PR1-103.34	0.08	Few bivalve shells fragments.	Continental to coastal marsh.
PR1-103.91	0.09	Few bivalve shells fragments.	Continental to coastal marsh.
PR1-108.5	17.98	Very rare planktic species: <i>N. pachyderma</i> .	Continental to transitional environment.
PR1-110.5	58.68	Very rare planktic species: <i>N. pachyderma</i> , <i>G. bulloides</i> .	Continental to transitional environment.

3.4. Paleomagnetic Data

3.4.1. Paleomagnetic Behavior

The NRM intensity ranges between 3.5×10^{-6} and 7.0×10^{-3} A/m, with a mean of 8.6×10^{-5} A/m. Through stepwise AF demagnetization, the ChRM component was isolated in 73% of the analyzed samples. The maximum angular deviation (MAD) values range from 0.61 to 18.1. Figure 6 illustrates the typical demagnetization behavior. Most samples exhibit a low-coercivity overprint, which was successfully removed at peak fields ≤ 10 mT. The inclinations of the ChRM allow for the identification of magnetozones. These are primarily defined by using at least two consecutive samples with inclinations significantly different from neighboring intervals (Figure 7). Only one interval contains an isolated sample (-22.71 m) with polarity opposite to the rest of the magnetozone.

The observed ChRM inclinations are steeper than the present-day geocentric axial dipole (GAD) inclination ($\pm 61^\circ$) at the site latitude. With the available data, we cannot exclude the possibility that the discrepancy may be associated to an unremoved overprint. Mean ChRM inclinations were separately calculated for normal and reverse polarity populations using the Arason-Levi inclination-only algorithm (Arason & Levi, 2010) as implemented in the PuffinPlot application (Lurcock & Florindo, 2019). The normal polarity samples have a mean inclination of 55.05° ($N = 16$; $\alpha 95 = 9.4^\circ$), while the reverse polarity samples have a mean inclination of -54.54°

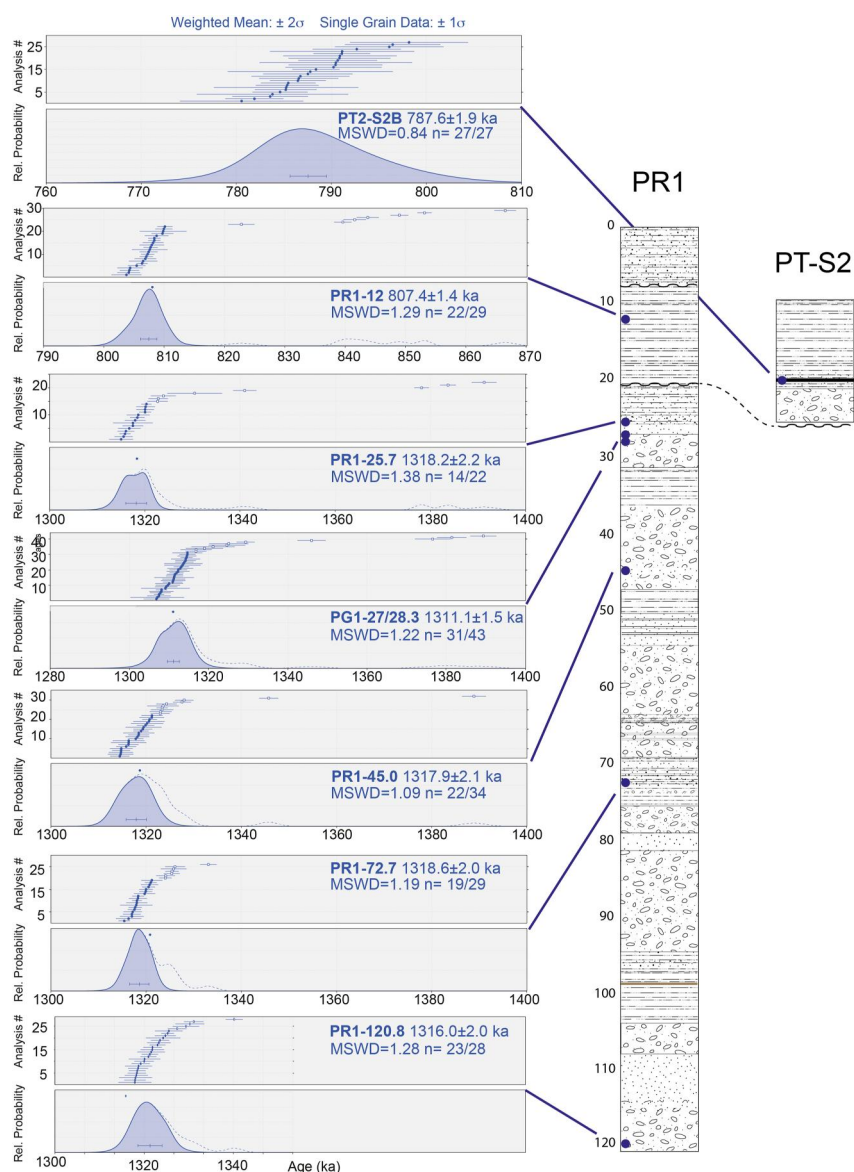


Figure 5. Relative probability diagrams showing crystal age distribution of the $^{40}\text{Ar}/^{39}\text{Ar}$ dated samples.

($N = 44$; $\alpha_{95} = 6.6^\circ$). These values pass the inclination-only reversals test at the 95% confidence level suggesting that the mean directions could indeed represent a reliable polarity record.

3.4.2. Magnetic Properties

Magnetic properties show some changes along the studied interval. The magnetic susceptibility ranges between 9.01×10^{-6} and 2.31×10^{-4} SI with a mean of 9.22×10^{-5} SI. The ARM parameter, which is particularly effective in activating finer magnetic grains, shows an average value of 7.7×10^{-4} A/m and ranges between 1.3×10^{-4} and 3.9×10^{-3} A/m (Figure 8). Downcore variations in magnetic susceptibility are associated with similar changes in ARM, suggesting that these fluctuations are primarily controlled by changes in magnetic mineral concentration. The highest values are found preferentially within the clays and sandy clay intervals.

Continuous monitoring of χ -T changes of samples above approximately -52 m reveals a maximum unblocking temperature between ca. 580 and 600°C, indicating the presence of magnetite (see details in Figure S9 in Supporting Information S1). The behavior of the discrete samples during AF demagnetization provides additional support for magnetite as the main magnetic carrier. The increase in susceptibility during cooling is likely due to

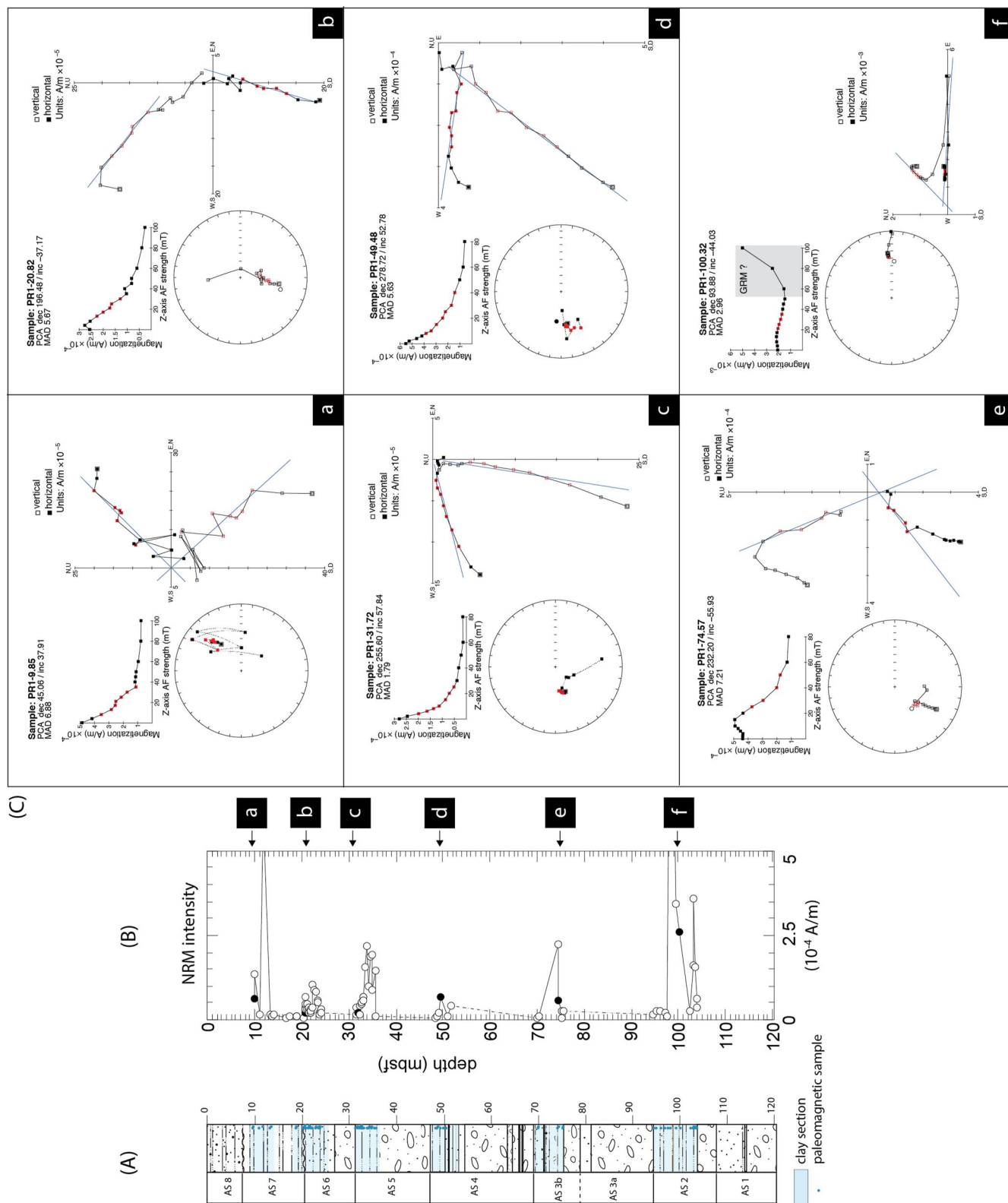


Figure 6. (a) Lithology, and (b) downcore variations of natural remanent magnetization (c) alternating field demagnetization behavior for six representative samples from Site PR1. For the vector component diagrams, open (closed) symbols represent projections onto the vertical (horizontal) plane. The blue lines represent linear regression fits that indicate the characteristic remanent magnetization (ChRM) direction for each sample. The stereoplots are equal area stereographic projections, where solid (open) symbols represent lower (upper) hemisphere projections. Samples are not azimuthally oriented and declinations are reported in the laboratory coordinate system with respect to the split face of the drill-core. PCA = principal component analysis. MAD = maximum angular deviation for the

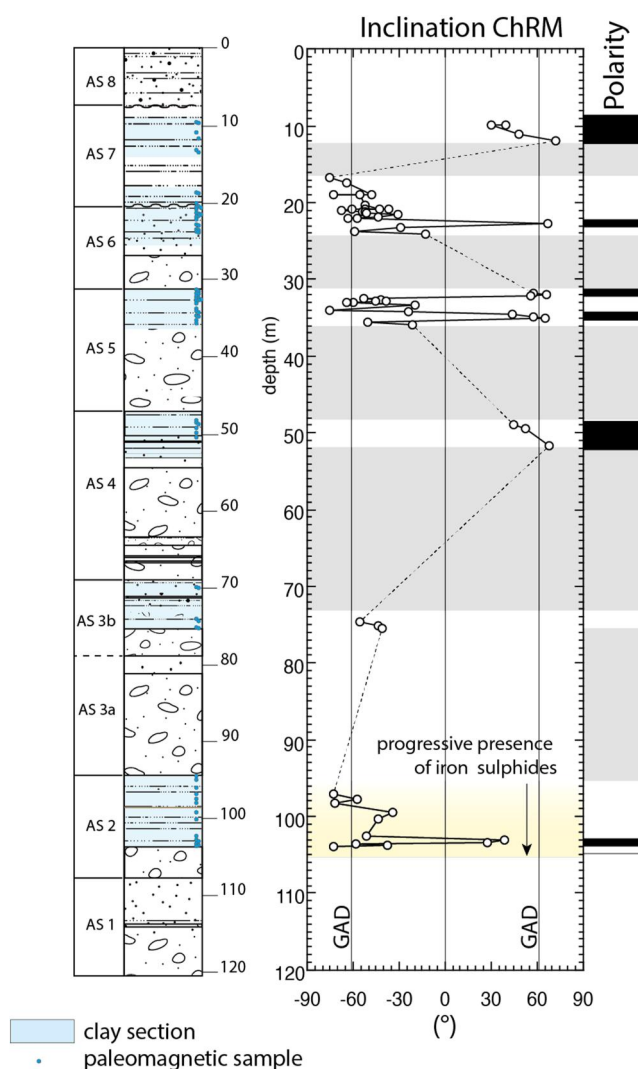


Figure 7. Lithology, downcore variations of characteristic remanent magnetization inclination and magnetic polarity zonation (black = normal polarity and white = reverse polarity). In gray, the intervals without samples are indicated.

the formation of ferrimagnetic minerals through the thermo-chemical alteration of paramagnetic clays. Additionally, hysteresis measurements showed a high concentration of paramagnetic minerals in these samples (see Figure S10 in Supporting Information S1).

Samples taken at depths below -75 m exhibit an increase in magnetic susceptibility around 370 – 400°C during heating, reaching peak susceptibility at approximately 470 – 500°C , followed by complete loss of magnetization (T_c) at around 570 – 600°C . The significant rise in susceptibility at approximately 370 – 400°C is likely attributed to the thermochemical alteration of weak magnetic iron sulfide minerals, such as pyrite, into magnetite.

The high M_{rs}/M_s values and low H_{cr}/H_c ratios of these samples (see Table S1 in Supporting Information S1) are indicative of ferrimagnetic iron sulphides, such as greigite (Roberts, 1995; Roberts et al., 2005, 2011). Although Roberts et al. (2018) highlighted some limitations of the Day plot for determining magnetic domain size, including the magnetic mineralogy, which was originally designed for magnetite and titanomagnetite, our study shows that the paleo-Tiber River sediments can be easily classified based on their mineralogy in the Day plot (Figure S11 in Supporting Information S1).

The behavior of some discrete samples during AF demagnetization provides additional support for the presence of magnetic iron sulfide. For some samples below -52 m, AF demagnetization above 50 mT was obscured by the

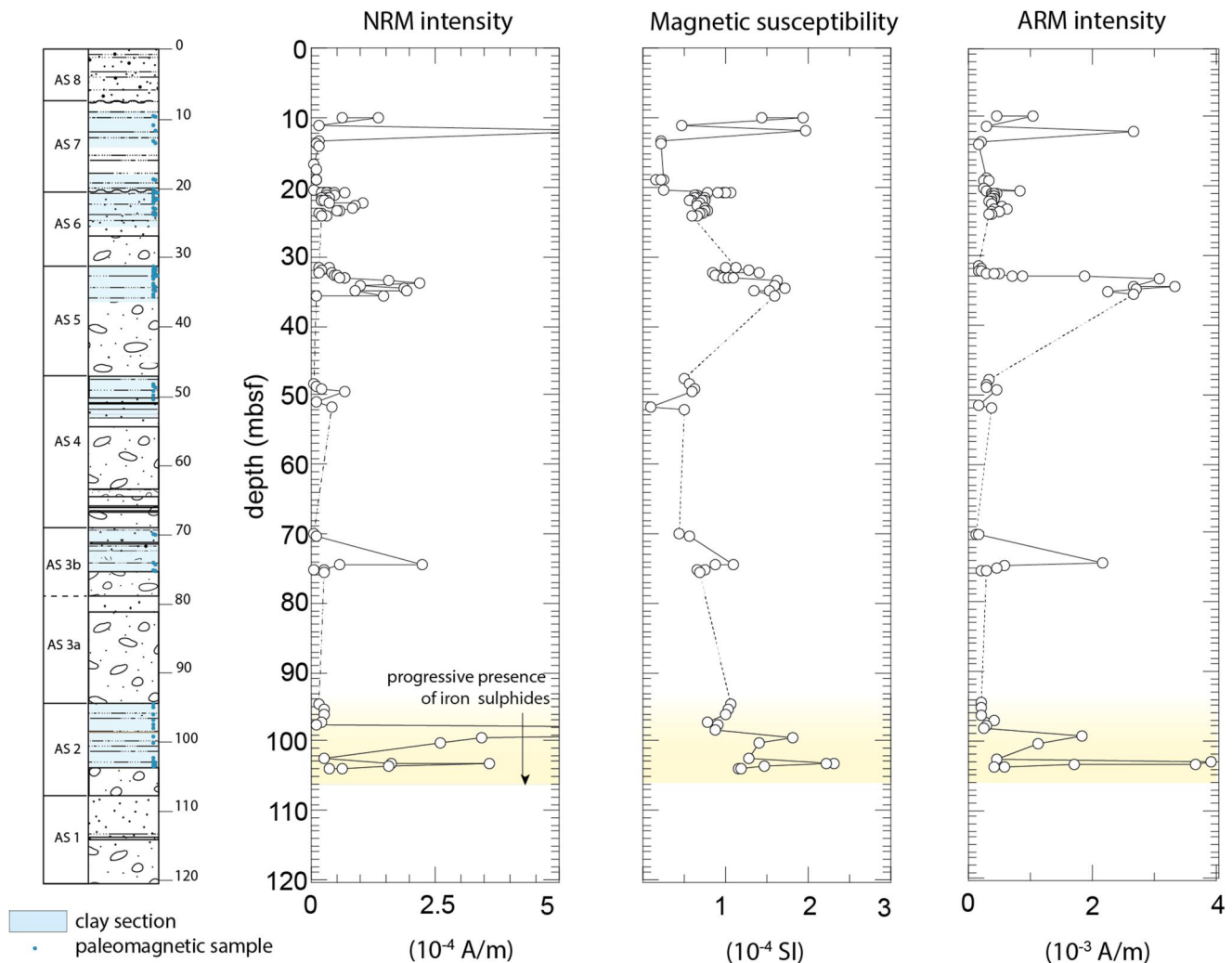


Figure 8. Lithology and downcore variation of the main magnetic properties.

simultaneous acquisition of a gyroremanent magnetization (GRM) (Stephenson, 1980, 1981) (e.g., sample -98.24 m). The presence of a GRM suggests the occurrence of single-domain material, and sedimentary greigite commonly exhibits single-domain-like properties (Roberts, 1995; Roberts et al., 2011).

In the previously studied sedimentary record of the MIS 19 aggradational succession of the Paleo-Tiber recovered in borecores PSA and VVM (Florindo et al., 2007), identified the presence of iron sulfides, including coarse-grained pyrite framboids and fine-grained (single domain) greigite in the clay samples. The fact that the PR1 record shows the presence of iron sulfide occurrences, possibly diagenetic greigite, limited only to the lower depths or at a few middepth intervals, is consistent with the observed transitional depositional environment of the lowest aggradational successions encountered in PR1. These are characterized by marine influences, in contrast to the pronounced continental features of the uppermost one, which correlates with the aggradational succession encountered in PSA and VVM boreholes.

4. Discussion

4.1. Micropaleontological Analyses

4.1.1. Interval 114–108 m (-86 m to -91 m)

The fine fraction of this oldest aggradational succession, represented by sand, is characterized on top by rare planktic foraminifers such as *G. bulloides* and *N. pachyderma* (Table 1). This could suggest an environment

characterized by a fluvial valley (or channel) being filled firstly by gravel, and subsequently by progressively finer sediments and occasionally being inundated by marine water which enabled the transport of such deep marine foraminifers from more distal, bathyal areas. In this case, even if a sea level rise can be deduced, finer sediments (clay) were never deposited, or were eroded during the subsequent lowstand. The planktic foraminifers identified are common species living for most of the Neogene and are found in present day plankton and consequently we do not have the basis to assume reworking from older layers.

4.1.2. Interval 104–94 m (–81 m to –71 m)

Here, the first signs of relative sea level rise are indicated by the progressive more consistent presence of marine benthic fauna (*V. bradyana*, *Elphidium spp.*, *C. lobatulus*, *A. planorbis*) typical of internal shelf (Olson & Leckie, 2003) and bivalve shells fragments (Table 1). This, paired with the presence of deepwater planktic foraminifers suggests that such faunal assemblage could be transported via the gradual transition further away from the river mouth and closer to the shore. The depositional environment after the gravel deposition was most probably a transitional environment, influenced both by fresh (organic matter of fluvial origin) and salty water. The lack of reworked or transported benthic species in the lowest two samples allows us to exclude that those occurring in the upper sample may derive from erosion of the older, Plio-Pleistocene marine substrate (“Monte Vaticano” Unit, Marra et al. (1995)). Indeed, microforaminifers deriving from reworked sediments of the older substrate, if present, should occur in all the samples. More in general, none of the characteristic, abundant planktonic species of the Monte Varicano Unit (e.g., *Globorotalia inflata*, *Globorotalia aemiliana*, *Globorotalia puncticulata* (Carboni, 1975; Marra et al., 1995)) are observed in the microforaminiferal assemblages of the investigated samples, ruling out a contribution of reworked planktic and benthic specimens from the older sedimentary substrate.

4.1.3. Interval 75–69.3 m (–53 m to –46.3 m)

In this sandy clay interval some rare benthic and planktic foraminifers appear. In sample PR1-74.95, together shallow water species (Murray (2006); from lagoon to neritic environments; *C. lobatulus* and *A. beccarii*) and deep water species (outer neritic and bathyal environments; *Nodosaria spp.*, *B. aculeata*, *C. laevigata*, *P. bulloides*, *Cibicides sp.*) can be found while organic matter and wood fragments are abundant (Table 1). In the following sample, deep water planktic and upper neritic to bathyal benthic foraminifers (Olson and Leckie (2003); Bulian et al. (2022) and references therein; *K. bradyi*, *Cibicides sp.*, *P. bulloides*, *Brizalina spp.*) prevail. Similarly as before, even in the absence of an open marine environment, the increase in marine influence is still evident, indicating a transitional environment, possibly a tidal channel or flat located on the deltaic plain. In this setting, there is a progressive increase in marine influxes, with more numerous deep benthic and planktic species being introduced from further offshore.

4.1.4. Interval 53.5 to 47.3 m (–30.5 to –24.3 m)

Considering the micropaleontological content of this sequence, and the sand content ranging between 15% and 20%, this interval was most likely characterized by a transitional environment closer to the coast (deltaic front) (Table 1). In fact, moving upwards through the sequence, it appears that we are transitioning away from the river mouth (from a delta plain to a delta front) and getting closer to the sea. This progression is evident through a reduction in organic matter, accompanied by higher abundances and diversity of transported deep-water planktic and benthic foraminifers. Nevertheless, the latter are found together with species, most likely in place, that are tolerant to lower salinities, such as the *Ammonia* group and *Rosalina spp.* found in lagoonal environments (Guelorget & Perthuisot, 1983; Murray, 2006), or *C. lobatulus*, an epiphytic taxon living attached to seagrass (Bolliet et al., 2014), in many instances developed in patches on delta front platforms or in the inter-distributary bays.

4.1.5. Interval 36.5 to 31.3 m (–13.5 to –8.3 m)

Sediment residue analyses suggest the development of a stagnant marsh or peat environment during this clay interval, indicated by high quantities of organic matter and the presence of ostracods, some bivalve and gastropods opercula (Table 1). Evidently, this interval was characterized by a more continental, fluvial influenced, coastal environment, evolving upward to a coastal alluvial plain.

4.1.6. Interval 26 to 20.8 m (−3 to 2.2 m)

The fining upward sand sequence, initially barren in fauna, progressively starts containing rare but well-preserved marine deep water planktic foraminifers, which become more diverse in the uppermost sample. In the latter shallow water species *C. lobatulus* and *A. tepida* also appear (Murray, 2006) (Table 1). This, paired with the high quantities of sand fraction (ca. 70%–40%) showing a fining upward pattern could suggest a progressive establishment of an area more proximal to the sea, like a delta front, or a distributary channel in the delta front where small shallow water embayments can form and where paired with the in situ shallow water taxa, deep planktic species could be transported. As all the foraminifer species found present throughout the entire Neogene and in the present-day plankton and benthos, and due to their good preservation, reworking from older sediments may be excluded.

4.1.7. Interval 20.8 to 7.7 (2.2–15.3 m)

A continental environment can be found in this horizon that culminates with the highly evaporative facies of sample PR1-16.5 which suggests a regressive phase that follows the highstand (Table 1). The marine environments immediately filled, and the delta started prograding rapidly changing this area from coastal-transitional area to a continental environment.

4.2. Correlation With the GITS and the $\delta^{18}O$ Record

The $^{40}Ar/^{39}Ar$ maximum depositional age of 807.4 ± 1.4 ka (sample PR1-12) and the paleomagnetic data from the AS7 clay section provide clear evidence for the correlation of the uppermost magnetozone with the Brunhes Chron (Figure 9). Based on the stratigraphic position of the B-M boundary and considering the terminus post quem provided by a maximum age of 1317 ± 1 ka (weighted mean age of the five underlying samples), we have identified the following sequence of events: Kamikatsura and Santa Rosa excursions, Jaramillo subchron, and Cobb Mountain subchron. The B-M transition occurring within the interval between 11.91 and 18.91 m combined with age of 807.4 ± 1.4 ka yielded by sample PR-12 provide unambiguous correlation of AS7 with MIS 19. These chronostratigraphic constraints confirm the previously inferred lateral stratigraphic correlation with the aggradational succession recovered in boreholes PT-S2 and PT-S6, in which the primary tephra layers dated 788 ± 2 ka (this work), 793 ± 13 ka, and 784 ± 13 ka (Florindo et al., 2007) are embedded (Figure 4). By combining these data with the terminus post quem provided by maximum age of 1317 ± 1 ka to the emplacement of the other ASs, we performed a correlation among AS6 to AS1 and each successive isotopic stage preceding MIS 19 in the $\delta^{18}O$ record. As a second step, we checked such correlation through the paleomagnetic signature of the investigated clay sections, obtaining a satisfactory match (Figure 9). The MIS 19 AS7 record the B-M transition and is characterized by sandy silt and sand with carbonatic concretions of fluvial-lacustrine environment. These sediments represent the late stages of sedimentation following the complete sea-level rise and the establishment of a near-coast alluvial plain. This scenario is consistent with the occurrence of the B-M transition shortly after the highstand (Figure 9). The sedimentary package including the basal gravel layer and the lower clay section which marks the glacial termination IX is missing at PR1 drilling site, due to its geomorphological features corresponding to a sector of higher elevation with respect to the bottom of the fluvial incision. The marked erosional contact with the underlying sandy clay section of AS6 accounts for the lack of a gravel layer, which is found at slightly lower elevation in the boreholes nearby (see cross-section in Figure 4). Notably, the normal polarity sample within the upper part of the AS6 clay section matches occurrence of the Kamikatsura excursion at 867 ka. Such geomagnetic event was previously re-assessed at 906 ka in a revision of the Geomagnetic Instability Time Scale (GITS) by Singer (2014); however, we speculate whether a distinct, 906 ka reversal actually occurred (dashed gray bar in Figure 9), consistent with the pair of normal polarity excursions occurring in the AS5 clay section.

A more problematic correlation is inferred between AS5 and the isotopic signal during MIS 25–23. Discussing on the direct proportionality between the isotopic ratio, ice volume and sea-level is beyond the scopes of the present work. We just remark on the subjectivity relying on assigning the status of isotopic stage to four peaks out of the five occurring between 900 and 1040 ka, which is not fitting neither their amplitude nor their recurrence. However, we think it is reasonable to assume that full glacial terminations only occurred during MIS 30/29 and MIS 26/25, due to the marked gain between the lowstand and the highstand. Based on this hypothesis, we correlate the AS5 clay section, recording two short events of normal polarity, with the two consecutive highstands

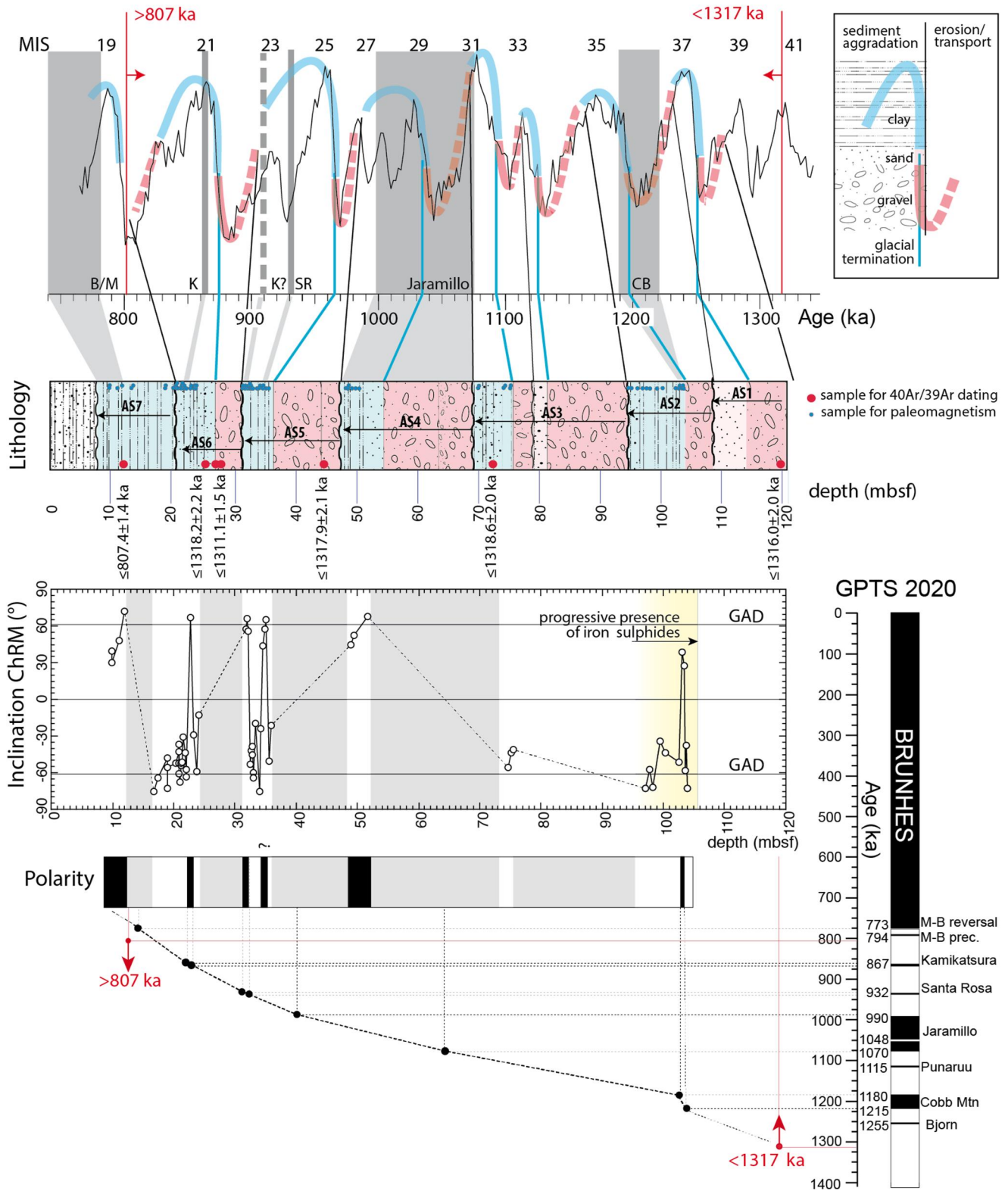


Figure 9. Correlation of the aggradational successions recovered in borehole PR1 and the sea-level oscillations detected by the $\delta^{18}\text{O}$ record, based on geochronologic and paleomagnetic constraints. See text for explanation.

of MIS 25 and MIS 23, which are not separated by a glacial termination. Therefore, we infer that the AS5 clay section represents a continuous sedimentary succession deposited during this whole-time span. Once this hypothesis is formulated, a striking match is observed between the two very close-in-time normal polarity intervals recorded in AS5 and the occurrence of the Santa Rosa excursion and the one previously identified as Kamikatsura, at 932 and 906 ka. A good match is observed between the normal polarity of the AS4 clay section and its correlation with the first two peaks of the MIS 29-MIS 27 interval, characterized by the occurrence of the late stages of the Jaramillo subchron. An intriguing correspondence is also found between the double feature of the AS3 gravel-sand/gravel-clay package and the two close MIS 33-MIS 31 highstands. The reversed polarity of the AS4 clay section further supports correlation with MIS 31 before the Jaramillo subchron. Another match supports correlation of AS2 with MIS 35, when the completion of the Cobb Mountain reversal at 1189 ka (Singer, 2014), soon after the glacial termination at the MIS 36/35 transition, is compared with the paleomagnetic signal recorded at the very initial stages of sediment aggradation. An alternative hypothesis that the observed reversal aligns with the older Bjorn excursion (1255 ka), and AS2 correlates with MIS 39 rather than MIS 37, appears unlikely. This is due to the improbable scenario of erasing the complete sedimentary record of a glacio-eustatic cycle. Additionally, the age of the Bjorn excursion predates the glacial termination at the beginning of MIS 39 and would not be captured by the clay section deposited during the sea-level rise. We cannot exclude, however, that the seemingly limited duration of the normal polarity interval in AS2 may result from the remagnetization of a portion of the sediment interval. The widespread presence of iron sulfides in the AS2 clay section has indeed been emphasized, potentially leading to later remagnetization during the subsequent reversed chron for the three samples collected at its base (Figure 9). Finally, the first AS1 recovered by PR1 borehole lacks of paleomagnetic constraints due to its coarse sedimentologic features; however, the maximum age of 1318 ka provided by sample PR1-120.8 and the assumed continuity of the sedimentary succession consent correlation with MIS 37.

4.3. Paleogeographic and Paleoclimatic Implications

Micropaleontological and sedimentologic analysis on the gravel-to-clay successions belonging to the AS1 through AS6 evidences their deposition in an environment which repeatedly evolved from continental, fluvial conditions to marine-influenced, coastal conditions. Such homogeneous features suggest that a delta of the Paleo-Tiber River was stably located in this area, 1250 to 850 ka, and that continuous subsidence, likely with a tectonic component, determined the deposition of a stacked package of aggradational successions during each glacio-eustatic cycle. In contrast, the marked continental features of AS7 are consistent with a SW progradation of the delta ~820 ka, as testified by geochronology and sedimentary data on the MIS 19 and MIS 17 ASs from the Ponte Galeria area near the Present coast (Marra et al., 1998; see Figure 1). Thickness of both the gravel and the clay sections vary in consequence of the intervening erosional phases, which partially to totally removed the preceding AS(s) and determined a lenticular shape for the gravel beds, resting on a variably incised bottom surface (see cross-section in Figure 4). However, probably the location at the center of the subsiding sector ("Paleotiber Graben"), consented the lucky circumstance allowing to recover a complete record of the sea-level oscillations, encompassing MIS 37 through MIS 19, in borehole PR1. Although, for the abovementioned reasons, no inference can be made on the absolute amplitude of the sea-level oscillations from the total thickness of each AS, an overall homogeneous feature for the glacio-eustatic cycles occurred 1250 through 870 ka is inferable. Moreover, the fact that the lowest AS recovered in PR1 between -85 and -97.8 m occurs at lower elevation with respect to the equivalent ones in other boreholes, which found the Plio-Pleistocene marine clay substrate at ca. -90 m, suggests the lack of older aggradational successions. The appearance of glacial-deglacial cycles, caused by the cyclic growth and decay of continental ice sheets in the Northern Hemisphere (NH), is commonly assumed around 2.8 Ma, with glacial intensification between 1.5 and 1.1 Ma, depending on the latitude at which the proxies of these events are located (Passchier (2018), and references therein). ODP Site 986 records major glacial expansion between 1.5 and 1.3 Ma (Butt et al., 2000), while at lower latitude, the oldest recorded glacial advance by the Scandinavian Ice Sheet onto the Norwegian Shelf is dated at 1.1 Ma (Sejrup et al., 2000). Based on surface exposure data, Balco and Rovey (2010) reconstruct major advances of the Laurentide Ice Sheet only from about 1.3 Ma. At high latitude, a persistent increase in sedimentation rates from 1.2 Ma onward is observed at IODP Site U1417 on the southern Alaska margin (Jaeger et al., 2014). The Paleo-Tiber delta data set of ASs suggests a significant input of glacio-eustacy on sedimentation processes also around 1.25 Ma in the Mediterranean Region.

5. Conclusions

The combined geochronologic and paleomagnetic constraints provided to the gravel and clay successions recovered in borehole PR1 consent an overall good correlation between each of the aggradational successions and each period of sea-level rise inferred from the $\delta^{18}O$ curve in the interval encompassing MIS 19 - MIS 37, 780 through 1250 ka. This stratigraphic record from the Paleo-Tiber delta provides a unique and well-dated evidence of the occurrence of glacial/deglacial events, strictly matching with the isotopic record in this time span. Results of this study confirm the hypothesis that gravel deposition in the catchment basin and the delta of the main rivers of central Italy is triggered by melting of the Apennines Mountain range glaciers, providing the water transport energy and a surplus of clastic input. Such hydrologic/sedimentary processes, which occur in any mountain region of the globe, if correctly depicted and dated, may provide a large data set of deglaciation proxies to unravel the chronology of glacio-eustatic events occurring during the last 2.8 Ma. In addition, the adopted innovative dating method based on “detrital sanidine” provides a means to extend the $^{40}Ar/^{39}Ar$ dating to sedimentary deposits, widening its potentiality to regions not directly affected by deposition of primary volcanics.

Data Availability Statement

Data generated during this study are openly available in PANGAEA (Florindo et al., 2023).

Acknowledgments

We express our gratitude to Jeff Benowitz, an anonymous reviewer, Associate Editor Agnes Kontry, and Editor Mark Dekkers for their insightful comments, which have enhanced the quality of the manuscript. This work received support from INGV funds.

References

- Alvarez, W., Ammerman, A. J., Renne, P. R., Karner, D. B., Terrenato, N., & Montanari, A. (1996). Quaternary fluvial-volcanic stratigraphy and geochronology of the Capitoline hill in Rome. *Geology*, 24(8), 751. [https://doi.org/10.1130/0091-7613\(1996\)024<0751:QFVSAG>2.3.CO;2](https://doi.org/10.1130/0091-7613(1996)024<0751:QFVSAG>2.3.CO;2)
- Arason, P., & Levi, S. (2010). Maximum likelihood solution for inclination-only data in paleomagnetism. *Geophysical Journal International*, 182(2), 753–771. <https://doi.org/10.1111/j.1365-246X.2010.04671.x>
- Balco, G., & Rovey, C. W. (2010). Absolute chronology for major Pleistocene advances of the Laurentide ice sheet. *Geology*, 38(9), 795–798. <https://doi.org/10.1130/G30946.1>
- Barberi, F., Buonasorte, G., Cioni, R., Fiordelisi, A., Foresi, L., Iaccarino, S., et al. (1994). Plio-Pleistocene geological evolution of the geothermal area of Tuscany and Latium. *Memorie Descrittive della Carta Geologica d'Italia*, 49, 77–134.
- Barker, S., Knorr, G., Conn, S., Lordsmith, S., Newman, D., & Thornalley, D. (2019). Early interglacial legacy of deglacial climate instability. *Paleoceanography and Paleoclimatology*, 34(8), 1455–1475. <https://doi.org/10.1029/2019PA003661>
- Bolliet, T., Jorissen, F. J., Schmidt, S., & Howa, H. (2014). Benthic foraminifera from Capbreton Canyon revisited; faunal evolution after repetitive sediment disturbance. *Deep Sea Research Part II: Topical Studies in Oceanography*, 104, 319–334. <https://doi.org/10.1016/j.dsr2.2013.09.009>
- Bulian, F., Kouwenhoven, T. J., Andersen, N., Krijgsman, W., & Sierro, F. J. (2022). Reflooding and repopulation of the Mediterranean sea after the Messinian salinity crisis: Benthic Foraminifera assemblages and stable isotopes of Spanish basins. *Marine Micropaleontology*, 176, 102160. <https://doi.org/10.1016/j.marmicro.2022.102160>
- Butt, F. A., Elverhøi, A., Solheim, A., & Forsberg, C. F. (2000). Deciphering late Cenozoic development of the western Svalbard margin from ODP site 986 results. *Marine Geology*, 169(3–4), 373–390. [https://doi.org/10.1016/S0025-3227\(00\)00088-8](https://doi.org/10.1016/S0025-3227(00)00088-8)
- Carboni, M. G. (1975). Biostratigrafia di alcuni affioramenti Pliocenici del versante tirrenico dell'Italia centrale. *Geologica Romana*, 14, 63–85.
- Florindo, F., Karner, D. B., Marra, F., Renne, P. R., Roberts, A. P., & Weaver, R. (2007). Radioisotopic age constraints for Glacial Terminations IX and VII from aggradational sections of the Tiber River delta in Rome, Italy. *Earth and Planetary Science Letters*, 256(1–2), 61–80. <https://doi.org/10.1016/j.epsl.2007.01.014>
- Florindo, F., & Marra, F. (1995). A revision of the stratigraphy for the middle Pleistocene continental deposits of Rome (Central Italy): Palaeomagnetic data. *Annals of Geophysics*, 38. <https://doi.org/10.4401/ag-4118>
- Florindo, F., Marra, F., Jicha, B., Bulian, F., Di Chiara, A., & Srivastava, P. (2023). Glacier melting triggers massive gravel deposition in central Italy's river basins, unveiling deglacial events from 1.25 to 0.78 Ma. [Dataset]. PANGAEA. <https://doi.org/10.1594/PANGAEA.963933>
- Giaccio, B., Marino, G., Marra, F., Monaco, L., Pereira, A., Zanchetta, G., et al. (2021). Tephrochronological constraints on the timing and nature of sea-level change prior to and during glacial termination V. *Quaternary Science Reviews*, 263, 106976. <https://doi.org/10.1016/j.quascirev.2021.106976>
- Giaccio, B., Regattieri, E., Zanchetta, G., Wagner, B., Galli, P., Mannella, G., et al. (2015). A key continental archive for the last 2 Ma of climatic history of the central Mediterranean region: A pilot drilling in the Fucino basin, central Italy. *Scientific Drilling*, 20, 13–19. <https://doi.org/10.5194/sd-20-13-2015>
- Giraudi, C., & Giaccio, B. (2017). Middle Pleistocene glaciations in the Apennines, Italy: New chronological data and preservation of the glacial record. *Geological Society of London Special Publications*, 433(1), 161–178. <https://doi.org/10.1144/SP433.1>
- Grant, K. M., Rohling, E. J., Ramsey, C. B., Cheng, H., Edwards, R. L., Florindo, F., et al. (2014). Sea-level variability over five glacial cycles. *Nature Communications*, 5(1), 5076. <https://doi.org/10.1038/ncomms6076>
- Guelorget, O., & Perthuisot, J. (1983). *Le domaine paraliqque: Expressions géologiques, biologiques et économiques du confinement*. Presses de l'École normale supérieure.
- Heizler, M. T., Karlstrom, K. E., Albonico, M., Hereford, R., Beard, L. S., Cather, S. M., et al. (2021). Detrital Sanidine $^{40}Ar/^{39}Ar$ dating confirms < 2 Ma age of Crooked Ridge Paleo river and subsequent deep denudation of the southwestern Colorado Plateau. *Geosphere*, 17(2), 438–454. <https://doi.org/10.1130/GES02319.1>
- Jaeger, J., Gulick, S., Le Vay, L., Asahi, H., Bahlburg, H., Belanger, C., et al. (2014). Expedition reports Southern Alaska margin. (Tech. Rep.). *Proceedings of the integrated ocean drilling program*, Vol. 341. Integrated Ocean Drilling Program.
- Jicha, B. R., Singer, B. S., & Sobol, P. (2016). Re-evaluation of the ages of $^{40}Ar/^{39}Ar$ sanidine standards and supereruptions in the western U.S. using a Noblesse multi-collector mass spectrometer. *Chemical Geology*, 431, 54–66. <https://doi.org/10.1016/j.chemgeo.2016.03.024>

- Karner, D. B., & Marra, F. (1998). Correlation of fluviodeltaic aggradational sections with glacial climate history: A revision of the Pleistocene stratigraphy of Rome. *GSA Bulletin*, 110(6), 748–758. [https://doi.org/10.1130/0016-7606\(1998\)110\(0748:COFASW\)2.3.CO;2](https://doi.org/10.1130/0016-7606(1998)110(0748:COFASW)2.3.CO;2)
- Karner, D. B., & Marra, F. (2003). $^{40}\text{Ar}/^{39}\text{Ar}$ dating of glacial termination V and the duration of Marine Isotopic Stage 11 (pp. 61–66). American Geophysical Union Geophysical Monograph Series. <https://doi.org/10.1029/137GM05>
- Karner, D. B., Marra, F., & Renne, P. R. (2001). The history of the Monti Sabatini and Alban hills volcanoes: Groundwork for assessing volcanic-tectonic hazards for Rome. *Journal of Volcanology and Geothermal Research*, 107(1–3), 185–219. [https://doi.org/10.1016/S0377-0273\(00\)00258-4](https://doi.org/10.1016/S0377-0273(00)00258-4)
- Karner, D. B., & Renne, P. R. (1998). $^{40}\text{Ar}/^{39}\text{Ar}$ geochronology of Roman volcanic province tephra in the Tiber River valley: Age calibration of middle Pleistocene sea-level changes. *Geological Society of America Bulletin*, 110(6), 740–747.
- Kirschvink, J. (1980). The least-squares line and plane and the analysis of palaeomagnetic data. *Geophysical Journal International*, 62(3), 699–718. <https://doi.org/10.1111/j.1365-246x.1980.tb02601.x>
- Kucera, M. (2007). Chapter six planktonic foraminifera as tracers of past oceanic environments. *Developments in Marine Geology*, 1, 213–262. [https://doi.org/10.1016/S1572-5480\(07\)01011-1](https://doi.org/10.1016/S1572-5480(07)01011-1)
- Lisiecki, L. E., & Raymo, M. E. (2005). A Pliocene-Pleistocene stack of 57 globally distributed benthic $\delta^{18}\text{O}$ records. *Paleoceanography*, 20(1), PA1003. <https://doi.org/10.1029/2004PA001071>
- Luberti, G. M., Marra, F., & Florindo, F. (2017). A review of the stratigraphy of Rome (Italy) according to geochronologically and paleomagnetically constrained aggradational successions, glacio-eustatic forcing and volcano-tectonic processes. *Quaternary International*, 438, 40–67. <https://doi.org/10.1016/j.quaint.2017.01.044>
- Lurcock, P. C., & Florindo, F. (2019). New developments in the PuffinPlot paleomagnetic data analysis program. *Geochemistry, Geophysics, Geosystems*, 20(11), 5578–5587. <https://doi.org/10.1029/2019GC008537>
- Marra, F., Bozzano, F., & Cinti, F. R. (2013). Chronostratigraphic and lithologic features of the Tiber River sediments (Rome, Italy): Implications on the post-glacial sea-level rise and Holocene climate. *Global and Planetary Change*, 107, 157–176. <https://doi.org/10.1016/j.gloplacha.2013.05.002>
- Marra, F., Carboni, M., Bella, L., Faccenna, C., Funicello, R., & Rosa, C. (1995). Il substrato plio-pleistocenico nell'area romana. *Bollettino della Società Geologica Italiana*, 114, 195–214.
- Marra, F., Ceruleo, P., Jicha, B., Pandolfi, L., Petronio, C., & Salari, L. (2015). A new age within MIS 7 for the Homo neanderthalensis of saccopastore in the glacio-eustatically forced sedimentary successions of the Aniene River Valley, Rome. *Quaternary Science Reviews*, 129, 260–274. <https://doi.org/10.1016/j.quascirev.2015.10.027>
- Marra, F., Costantini, L., Di Buduo, G. M., Florindo, F., Jicha, B. R., Monaco, L., et al. (2019). Combined glacio-eustatic forcing and volcano-tectonic uplift: Geomorphological and geochronological constraints on the Tiber River terraces in the eastern Vulsini Volcanic District (central Italy). *Global and Planetary Change*, 182, 103009. <https://doi.org/10.1016/j.gloplacha.2019.103009>
- Marra, F., & Florindo, F. (2014). The subsurface geology of Rome: Sedimentary processes, sea-level changes and astronomical forcing. *Earth-Science Reviews*, 136, 1–20. <https://doi.org/10.1016/j.earscirev.2014.05.001>
- Marra, F., Florindo, F., & Boschi, E. (2008). History of glacial terminations from the Tiber River, Rome: Insights into glacial forcing mechanisms. *Paleoceanography*, 23(2), PA2205. <https://doi.org/10.1029/2007PA001543>
- Marra, F., Florindo, F., & Jicha, B. R. (2017). $^{40}\text{Ar}/^{39}\text{Ar}$ dating of glacial termination VI: Constraints on the duration of marine isotopic stage 13. *Scientific Reports*, 7(1), 8908. <https://doi.org/10.1038/s41598-017-08614-6>
- Marra, F., Florindo, F., & Karner, D. B. (1998). Paleomagnetism and geochronology of early middle Pleistocene depositional sequences near Rome: Comparison with the deep-sea $\delta^{18}\text{O}$ record. *Earth and Planetary Science Letters*, 159(3), 147–164. [https://doi.org/10.1016/S0012-821X\(98\)00071-5](https://doi.org/10.1016/S0012-821X(98)00071-5)
- Marra, F., Gaeta, M., Jicha, B. R., Nicosia, C., Tolomei, C., Ceruleo, P., et al. (2019). MIS 9 to MIS 5 terraces along the Tyrrhenian Sea coast of Latium (central Italy): Assessing interplay between sea-level oscillations and tectonic activity. *Geomorphology*, 346, 106843. <https://doi.org/10.1016/j.geomorph.2019.106843>
- Marra, F., Pereira, A., Boschian, G., & Nomade, S. (2021). MIS 13 and MIS 11 aggradational successions of the Paleo-Tiber delta: Geochronological constraints to sea-level fluctuations and to the Acheulean sites of Castel di Guido and Malagrotta (Rome, Italy). *Quaternary International*, 616, 1–11. <https://doi.org/10.1016/j.quaint.2021.12.016>
- Marra, F., Pereira, A., Jicha, B., Nomade, S., Biddittu, I., Florindo, F., et al. (2022). Terrestrial records of deglaciation events during terminations V and IV in the central Apennines (Italy) and insights on deglacial mechanisms. *Scientific Reports*, 12(1), 18770. <https://doi.org/10.1038/s41598-022-23391-7>
- Marra, F., Rohling, E. J., Florindo, F., Jicha, B., Nomade, S., Pereira, A., & Renne, P. R. (2016). Independent $^{40}\text{Ar}/^{39}\text{Ar}$ and ^{14}C age constraints on the last five glacial terminations from the aggradational successions of the Tiber River, Rome (Italy). *Earth and Planetary Science Letters*, 449, 105–117. <https://doi.org/10.1016/j.epsl.2016.05.037>
- Marra, F., & Rosa, C. (1995). Stratigrafia e assetto geologico dell'area romana. *Memorie Descrittive della Carta Geologica d'Italia*, 50, 49–118.
- Murray, J. W. (2006). *Ecology and applications of benthic foraminifera*. Cambridge University Press. <https://doi.org/10.1017/CBO9780511535529>
- Olson, H. C., & Leckie, R. M. (2003). Micropaleontologic proxies for sea-level change and stratigraphic discontinuities. *SEPM Society for Sedimentary Geology*. <https://doi.org/10.2110/pec.03.75>
- Passchier, S. (2018). Chapter 16—Ice sheets and climate: The marine geological record. In J. Menzies & J. J. van der Meer (Eds.), *Past glacial environments* (pp. 565–584). Elsevier. <https://doi.org/10.1016/B978-0-08-100524-8.00017-8>
- Peccerillo, A. (2017). *Cenozoic volcanism in the Tyrrhenian Sea region*. Springer. <https://doi.org/10.1007/978-3-319-42491-0>
- Pereira, A., Monaco, L., Marra, F., Nomade, S., Gaeta, M., Leicher, N., et al. (2020). Tephrochronology of the central Mediterranean MIS 11c interglacial (425–395 ka): New constraints from the Vico volcano and Tiber delta, central Italy. *Quaternary Science Reviews*, 243, 106470. <https://doi.org/10.1016/j.quascirev.2020.106470>
- Roberts, A. P. (1995). Magnetic properties of sedimentary Greigite (Fe₃S₄). *Earth and Planetary Science Letters*, 134(3), 227–236. [https://doi.org/10.1016/0012-821X\(95\)00131-U](https://doi.org/10.1016/0012-821X(95)00131-U)
- Roberts, A. P., Chang, L., Rowan, C. J., Horng, C.-S., & Florindo, F. (2011). Magnetic properties of sedimentary Greigite (Fe₃S₄): An update. *Reviews of Geophysics*, 49(1), RG1002. <https://doi.org/10.1029/2010RG000336>
- Roberts, A. P., Jiang, W., Florindo, F., Horng, C., & Laj, C. (2005). Assessing the timing of Greigite formation and the reliability of the Upper Olduvai polarity transition record from the Crostolo River, Italy. *Geophysical Research Letters*, 32(5). <https://doi.org/10.1029/2004GL022137>
- Roberts, A. P., Tauxe, L., Heslop, D., Zhao, X., & Jiang, Z. (2018). A critical appraisal of the “Day” diagram. *Journal of Geophysical Research: Solid Earth*, 123(4), 2618–2644. <https://doi.org/10.1002/2017JB015247>

- Sejrup, H., Larsen, E., Landvik, J., King, E., Haflidason, H., & Nesje, A. (2000). Quaternary glaciations in southern Fennoscandia: Evidence from southwestern Norway and the northern north sea region. *Quaternary Science Reviews*, *19*(7), 667–685. [https://doi.org/10.1016/S0277-3791\(99\)00016-5](https://doi.org/10.1016/S0277-3791(99)00016-5)
- Singer, B. S. (2014). A Quaternary geomagnetic instability time scale. *Quaternary Geochronology*, *21*, 29–52. <https://doi.org/10.1016/j.quageo.2013.10.003>
- Stephenson, A. (1980). A gyroremanent magnetisation in anisotropic magnetic material. *Nature*, *284*(5751), 49–51. <https://doi.org/10.1038/284049a0>
- Stephenson, A. (1981). Gyroremanent magnetization in a weakly anisotropic rock sample. *Physics of the Earth and Planetary Interiors*, *25*(2), 163–166. [https://doi.org/10.1016/0031-9201\(81\)90149-7](https://doi.org/10.1016/0031-9201(81)90149-7)
- Van der Zwaan, G. J., Duijnstee, I. A. P., den Dulk, M., Ernst, S. R., Jannink, N. T., & Kouwenhoven, T. J. (1999). Benthic foraminifers: Proxies or problems? A review of paleocological concepts. *Earth-Science Reviews*, *46*(1), 213–236. [https://doi.org/10.1016/S0012-8252\(99\)00011-2](https://doi.org/10.1016/S0012-8252(99)00011-2)
- Villa, P., Soriano, S., Grün, R., Marra, F., Nomade, S., Pereira, A., et al. (2016). The Acheulian and early middle Paleolithic in Latium (Italy): Stability and innovation. *PLoS One*, *11*(8), e0160516. <https://doi.org/10.1371/journal.pone.0160516>